Journal of Structural Geology, Vol. 12, No. 5/6, pp. 667 to 684, 1990
Printed in Great Britain

0191-8141/90 $03.00 + 0.00

A barometric response to late compression in the Strangways Metamorphic Complex, Arunta Block, central Australia

A. R. NORMAN and G. L. CLARKE*

School of Earth Sciences, Macquarie University, Sydney, NSW 2109, Australia

(*Received* 10 *February* 1989; *accepted in revised form* 9 *February* 1990)

Abstract—Evidence for four major deformation events (D_1–D_4) and two metamorphic events (M_1, M_2) is shown by granulite- and amphibolite-facies rocks of the Strangways Metamorphic Complex, central Australia, which is divided into two domains: the Ongeva Granulites to the east, and the Anamarra Granite domain to the west. D_1 and D_2 produced layer-parallel foliations, with many of the effects of D_1 overprinted by intense non-coaxial shear during D_2. Low-pressure granulite-facies metamorphism, M_1, accompanied D_{1-2}, at conditions of $P = 5.3 \pm 1.2$ kbar and $T > 750$°C. The effects of M_1 are characterized by S_1 spinel + quartz-bearing assemblages, with overprinting S_{2b} sillimanite + biotite + magnetite assemblages, implying approximately isobaric cooling. Effects of M_2 are characterized by S_{1-2} cordierite pseudomorphed by orthopyroxene + sillimanite + biotite + magnetite symplectites, at conditions of $P = 7.5 \pm 0.8$ kbar and $T \cong 800$°C. This retrograde *increase* in pressure was probably the result of crustal thickening during D_3, which produced NE-plunging F_3 and F_4 folds in the Ongeva Granulites, and a widespread shear foliation in the Anamarra Granite domain. The increase in pressure with M_2 may reflect the beginning of a clockwise *P–T–t* path typical of collisional-style tectonics. Sillimanite and orthopyroxene-bearing ultramylonites were produced during D_4, an extension event parallel to the D_3 transport axis and probably related to crustal collapse after thickening during D_3.

Wide N-dipping shear zones (D_5) containing sillimanite, kyanite, staurolite and overprinting greenschist-facies assemblages bound the Strangways Metamorphic Complex. These zones indicate a S-directed sense of shear and were probably responsible for bringing the Strangways Metamorphic Complex to higher crustal levels, during both a probable late Proterozoic event and the Mid Carboniferous Alice Springs Orogeny.

INTRODUCTION

HIGH-GRADE Precambrian terrains dominate the continental fragments of Gondwana, and record the tectonic events that could be responsible for the formation of the supercontinent. However, the geological setting of these Precambrian tectonic events is commonly obscured by dislocation during much younger, unrelated tectonic events. In the absence of observed basement and/or tectonic margins, the deformation history of a terrain may be preserved in superimposed mineral fabrics, and the pressure–temperature (*P–T*) history preserved in the overprinting mineral assemblages that constitute such mineral fabrics. The metamorphic–deformation history may be expressed as a *P–T*–time (*t*) path, with the absolute timing of events constrained by geochronology. In such terrains, the timing of the thermal peak of metamorphism, with respect to deformation, provides a critical basis for assessing the tectonic setting of a deformation event. However, tectonic interpretations in many granulite-facies Precambrian terrains are weakened because the intensity of deformation and recrystallization has destroyed fabrics that pre-date the last metamorphism–deformation.

Models for the tectonic setting of regional metamorphism in the Phanerozoic usually invoke continental collision: intense sub-horizontal and upright foliations, geometrically specific to the axis of convergence (Shackleton & Ries 1984), reflect the deformation processes that result in crustal overthickening and metamorphism (e.g. Le Fort 1975, Caby *et al.* 1983, Windley 1985). The mountain belt is assembled in less than the thermal time constant of the lithosphere (England & Richardson 1977), and the agency by which metamorphism is terminated may be erosion (England & Richardson 1977) or extension (England 1987). Post-collisional thermal history for the assembled mountain belt may be complex (e.g. Sandiford in press) but a common inference made from rock fabrics is that compressive deformation precedes both the thermal peak of metamorphism and an essentially isothermal uplift (e.g. Selverstone *et al.* 1984) that returns the rocks to the Earth's surface. Thus a *'clockwise' P–T–t path* is inferred.

Problems in extrapolating a collisional tectonic setting to account for many granulite-facies Precambrian terrains include the thermally perturbed nature of the peak metamorphism, and the common inference that deformation, which is usually compressive (e.g. Clarke *et al.* 1986), occurred during cooling at constant, or slightly increasing, pressure (e.g. Phillips & Wall 1981, Warren 1983, Clarke *et al.* 1987, 1989, Harley 1989). Either *isobaric cooling* or an *'anticlockwise' P–T–t path* is inferred, where the peak of metamorphism preceded significant compressive deformation, and the terrain remained at depth subsequent to metamorphism (Harley 1989). In places, isograds of Precambrian metamorphism/deformation can be mapped (e.g. Hobbs *et al.* 1984), from which it is evident that the deformation events resulted in a locally complex, but regionally minimal, disruption to stratigraphy or regional geology (e.g. Clarke *et al.* 1986, 1989, 1990). Such effects should be contrasted with the 100 km displacements observed in Phanerozoic collisional orogens (e.g.

* Present address: Department of Geology and Geophysics, University of Sydney, NSW 2006, Australia.

LeFort 1975). Though simple isobaric cooling may reflect several tectonic settings (Sandiford & Powell 1986, Ellis 1987, Harley 1989), isobaric cooling during major compressive deformation is more probably part of an anticlockwise P–T–t path. An anticlockwise P–T–t path seems best explained by either passive crustal thickening subsequent to crustal extension (Stüwe & Powell 1989a) or by thermally weakened crust responding to existing regional stresses (G. L. Clarke & R. Powell unpublished data). Such settings involve the access of abnormal amounts of heat from local felsic intrusions or mafic magmas in the lower crust, from crustal extension (Sandiford & Powell 1986) or from fluid advection (Wells 1980, Thompson & Ridley 1987, Vernon *et al.* in press).

In assessing the tectonic setting of any observed deformation fabric, it is critical to establish the overprinting mineral assemblages. In this paper, we present the tectonic evolution of a portion of the central Australian Arunta Block, an extensive exposure of multiply deformed and metamorphosed Proterozoic rock (Noakes 1953). By relating the observed mineral assemblages to the rock fabrics, we infer that the rocks record both styles of P–T–t path outlined above and thus show overprinting metamorphisms of different tectonic setting. Evidence is presented for an earlier, low-pressure metamorphism (M_1) that probably corresponds to a widely reported early Proterozoic granulite-facies event (Black *et al.* 1983, Warren 1983) and a subsequent retrograde moderate-pressure metamorphism (M_2). We present evidence for a significant increase in pressure during M_2 which is linked to a widespread folding episode (D_3).

Mineral abbreviations used in figures and tables: ab—albite; alm—almandine; ann—annite; anth—anthophyllite; bi—biotite; chl—chlorite; crd—cordierite; east—eastonite; en—enstatite; ep—epidote; fcrd—Fe cordierite; fs—ferrosilite; g—garnet; ged—gedrite; herc—hercynite; il—ilmenite; kf—K-feldspar; ks—orthoclase; ky—kyanite; mei—meionite; mgts—Mg-Tschermak; mt—magnetite; musc—muscovite; naph—Na phlogopite; opx—orthopyroxene; phl—phlogopite; py—pyrope; q—quartz; ru—rutile; sill—sillimanite; sp—spinel.

REGIONAL GEOLOGY

The area under investigation is situated about 100–150 km northeast of Alice Springs, in rocks of the Lower Proterozoic Strangways Metamorphic Complex. These rocks form a part of the Arunta Block, which has been subdivided into three tectonostratigraphic Divisions (Stewart *et al.* 1984), and is unconformably overlain by Proterozoic to Phanerozoic basin sediments (Fig. 1). The Strangways Metamorphic Complex was multiply deformed and metamorphosed at granulite-facies conditions before being extensively dissected by mylonite and retrograde shear zones (Shaw *et al.* 1979, Shaw & Langworthy 1984) that subdivide the Complex into a number of spatially-independent, morphologic units (Fig. 1). The geology of the area is shown in Fig. 1, and the relationship between deformation and metamorphic events is shown in Table 1. We review the geology of the distinct morphological units, correlating tectonic events where appropriate.

The Strangways Metamorphic Complex forms part of the Division 1 rocks of Stewart *et al.* (1984) and are thought to record the oldest metamorphic event in the Arunta Block (~1800 Ma, Black *et al.* 1983) and a crustal formation age of about 2000 Ma (Windrim & McCulloch 1986). The first regional mapping of the area was by Joklik (1955), who used the term "Harts Range Group" for all the rocks north of the Hale River. However, following Shaw *et al.* (1984), we separate the area into two major units: the Harts Range Group to the north of, and Strangways Metamorphic Complex south of, the Gough Dam Schist Zone (Fig. 1). These units are broadly equivalent to the Harts Range Cover and Strangways Orogenic Belt, respectively, of Ding & James (1985) and James & Ding (1988), from work east of the area. We further divide the rocks of the Strangways Metamorphic Complex into the Ongeva Granulites (after Shaw *et al.* 1984) in the east, and the Anamarra Granite domain to the west.

Ongeva Granulites

The Ongeva Granulites consist of interlayered quartz + feldspar ± orthopyroxene ± garnet + biotite gneisses, two pyroxene + hornblende + plagioclase granofelses, quartz + K-feldspar + sillimanite + garnet + biotite gneisses and minor calc-silicate rocks and marble. The macroscopic compositional layering is here defined as S_1, as there is no evidence of bedding. These rocks record three major folding episodes (F_2–F_4) subsequent to a high-temperature, low-pressure, granulite-facies metamorphism (M_1) and followed by high-grade mylonitization (D_4, Table 1). Anatexis accompanied the granulite-facies metamorphism. Evidence of an S_1 metamorphic foliation has been largely obliterated in metapelites and felsic gneisses because of recrystallization by a non-coaxial ductile deformation, D_2, which produced the pervasive S_2 foliation, shown as trend lines in Fig. 1. Fine-grained sillimanite inclusions and inclusions of spinel in granoblastic cordierite and garnet are folded (F_2) and define an S_1 foliation in metapelites. In mafic rocks, S_1 layers contain medium-grained pyroxene + hornblende + plagioclase and are folded by F_2 folds. An S_{2a} foliation is defined by abundant, medium-grained quartz + K-feldspar leucosome in metapelitic rocks, and coarse-grained hornblende and orthopyroxene in thin plagioclase-rich leucosomes in metabasic gneisses; it is axial planar to rootless, intrafolial, isoclinal F_2 folds (Fig. 2a). Boudinage of coarse-grained D_1 leucosome and mafic layers is common in the S_{2a} foliation. S_{2a} is mostly subparallel to the compositional layering (S_1), but locally oblique. F_2 fold axes are difficult to measure and an L_2 mineral-elongation lineation is rare, due to later recrystallization; where it exists, it is generally subparallel and plunges to the southeast.

In metapelitic gneisses, a coarse-grained, sillimanite + biotite foliation cuts the main S_{2a} quartz + K-feldspar leucocratic layering (Fig. 2b), but is generally sub-

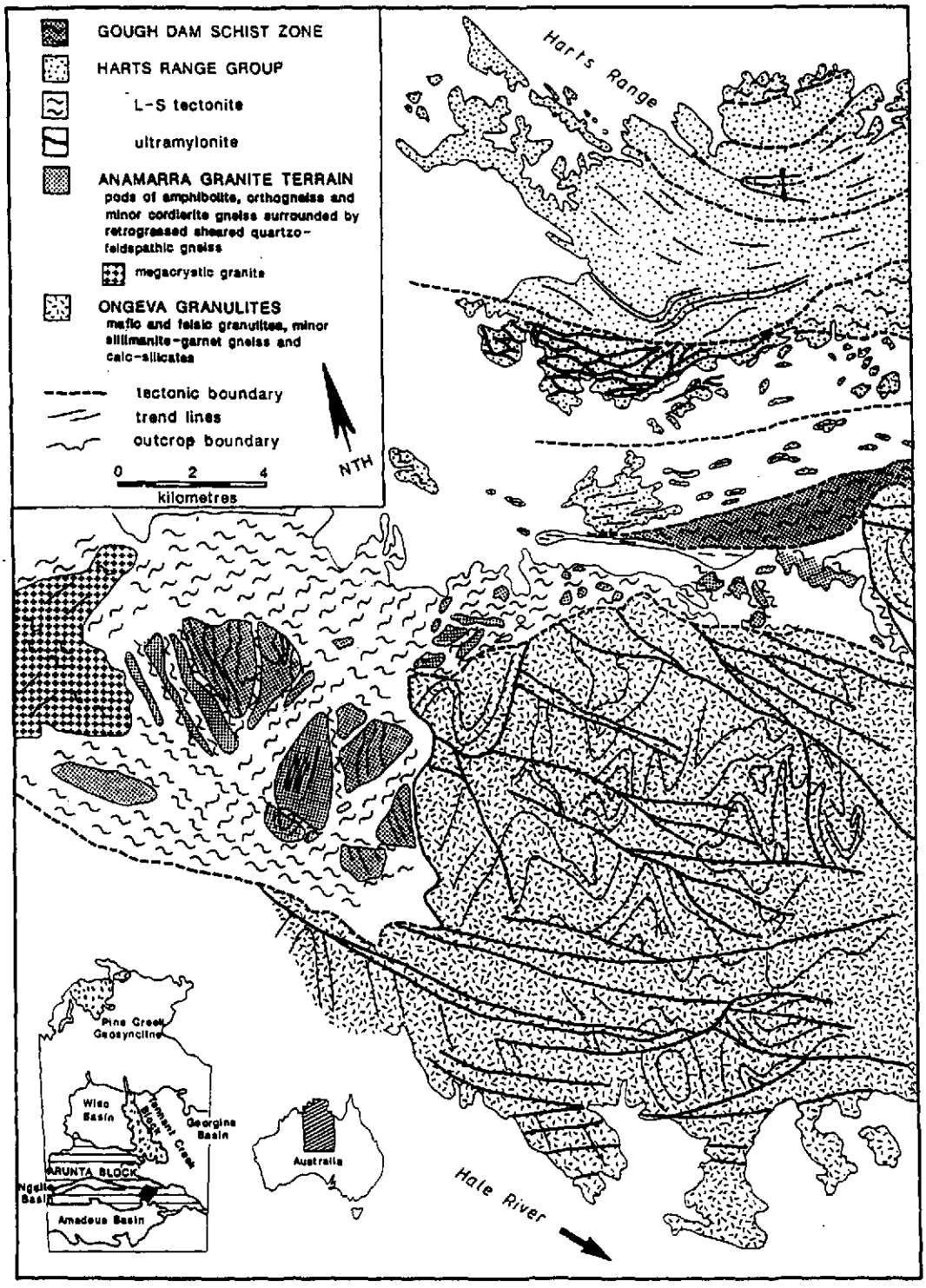

Fig. 1. Geological map of an area south of the Harts Range showing the Ongeva Granulites and the Anamarra Granite Domain.

parallel to the overall trend of S_{2a}, and is folded by tight to isoclinical F_3 folds. This foliation is here designated S_{2b}. Sillimanite in this foliation is poorly lineated, probably reflecting a flattening strain rather non-coaxial shear late in D_2. Large, irregularly-shaped, coarse-grained pegmatitic pods of garnet + K-feldspar + quartz + biotite (Fig. 2c) cut this sillimanite foliation and, in places, contain a poorly developed biotite foliation that is also parallel to S_2. Coarse-grained orthopyroxene-bearing pegmatitic pods in felsic granulites, and irregular networks of plagioclase + hornblende in mafic granulites (Fig. 2d) also cut the S_{2a} leucocratic foliation. In places, these coarse-grained pegmatitic pods occur between boudins on the limbs of early D_3 mylonitic folds. These relationships are inferred to represent the crystallization of melt late in D_2 and early in D_3, probably as a response to cooling from peak metamorphism (M_1).

The S_2 foliation, including leucosome crystallized from partial melt, is folded by NE-plunging, discontinuous, tight to isoclinal F_3 folds (Figs. 2e & f). F_3 folds are

Table 1. Summary of the deformation history of the Strangways Metamorphic Complex, showing the correlation between deformation and metamorphic events

Deformation	Folding events	Metamorphic events	Parageneses +kf + q + melt	Interpreted age constraints	Suggested correlation of events with Warren (1983)
D_1	F_1	M_1 $P = 5.5 \pm 0.8$ kbar $T > 750$°C	sill + sp + il ± g ± crd	1860 ± 80 Ma* 1790 ± 35 Ma†	**Granulite stage** $P = 8 \pm 1$ kbar, $T = 850$–920°C
D_2	F_2 isoclinal, intrafolial, rootless folds		crd + g + sill ± sp sill + bi + mt (S_{2b}) ± g		
D_3	F_3, F_4 isoclinal and open inclined, NW-verging				isobaric cooling
	NW-trending shear foliation in Anamarra Granite Domain	M_2 $P = 7.5 \pm 0.8$ kbar $T \cong 800$°C	opx + sill + bi + mt symplectite	1470 ± 60 Ma*	**Biotite stage**
D_4	North-side-down ultramylonitization		sill + bi ± g opx + bi ± g		
D_5	Southward directed thrusting within the Harts Range Group		ky ± sill ± st, ged-anth	1750 Ma‡§ 1450–1400 Ma†‖ 1000 Ma¶	**Kyanite–gedrite stage** $P \sim 8$ kbar $T = 650$–720°C Then isothermal uplift of 3–4 km, crd coronas to ky and sill **Cordierite–kyanite–gedrite stage**
			musc ± ep ± chl	mid-Carboniferous**	Terrain remained at depth until Alice Springs Orogeny

* Iyer *et al.* (1976); † Black *et al.* (1983); ‡ Mortimer *et al.* (1987); § Cooper *et al.* (1988); ‖ Allen & Stubbs (1982); ¶ Windrum & McCulloch (1986); ** Collins & Teyssier (1989).

refolded by open plunging inclined asymmetric F_4 folds (Fig. 2g). F_3 and F_4 folds are colinear, and both have a NW vergence, suggesting that they were the product of a single deformation event, here designated D_3. A mylonitic quartz foliation (S_3), and some quartz + K-feldspar ± garnet leucosomes are axial planar to F_3 folds in metapelitic gneisses. L_3 is evident as a quartz stretching lineation, which is parallel everywhere to F_3 fold axes and plunges at moderate angles to the NNE to NE. An axial-planar foliation is not well developed in the open F_4 folds, although a poorly developed quartz elongation lineation (L_4) is parallel to the F_4 fold axes and subparallel to the L_3 stretching lineation. Minor quartz + K-feldspar leucosome crystallized in conjugate shear sets on the limbs of F_4 folds, indicating the continual crystallization of leucosome from melt throughout D_3. F_4 folds are cut by quartz + K-feldspar + biotite pegmatities, which contain biotite elongate parallel to the F_4 axial plane and are deformed by subsequent mylonitization (D_4). A late D_3 pegmatite contains xenoliths derived from adjacent metapelites with assemblages associated with M_2 metamorphism (Fig. 5), implying that M_2 occurred before F_4 folding.

D_4 is characterized by narrow E-trending discrete zones of high-grade ultramylonite, which have a consistent north-side-down sense of shear and displace F_3 and F_4 folds (Norman 1989). The Strangways Metamorphic Complex is bound to the north and south by wide retrograde shear zones (D_5), which record southward thrusting. The D_4 ultramylonite zones appear to extend into the Anamarra Granite Domain and D_5 zones that bound the Strangways Metamorphic Complex contain sillimanite, kyanite and anthophyllite assemblages described by Warren (1983).

Anamarra Granite Domain

The Anamarra Granite Domain contains blocks of amphibolites, quartz-rich felsic gneisses, minor cordierite gneisses and mafic granulites enclosed in pervasively sheared quartzofeldspathic rock with minor biotite schist. This domain may represent a meta-igneous complex of largely granitic rocks with minor pods of metagabbro, which was intruded into gneisses of the Ongeva Granulites and was later deformed in D_3 and D_4.

The pods of high-grade gneiss contain numerous granite layers with K-feldspar megacrysts. Megacrystic granite is not observed in the Ongeva Granulites to the east. The mesoscopic layering and outcrop pattern of meta-igneous amphibolite and quartzofeldspathic gneisses in the Anamarra Granite Domain is very irregular. Three mesoscopic folding phases can be recognized, in the high-grade cordierite gneisses enclosed in the shear foliations, which are similar to F_2–F_4 in the Ongeva Granulites, although macroscopic fold patterns are not evident due to extensive dissection by sheared quartzo-feldspathic gneisses. An S_1 cordierite foliation is boudinaged and isoclinally folded by F_2, with quartz + K-feldspar + cordierite leucosome from melt in S_2, similar to the S_{2a} leucocratic layers in the

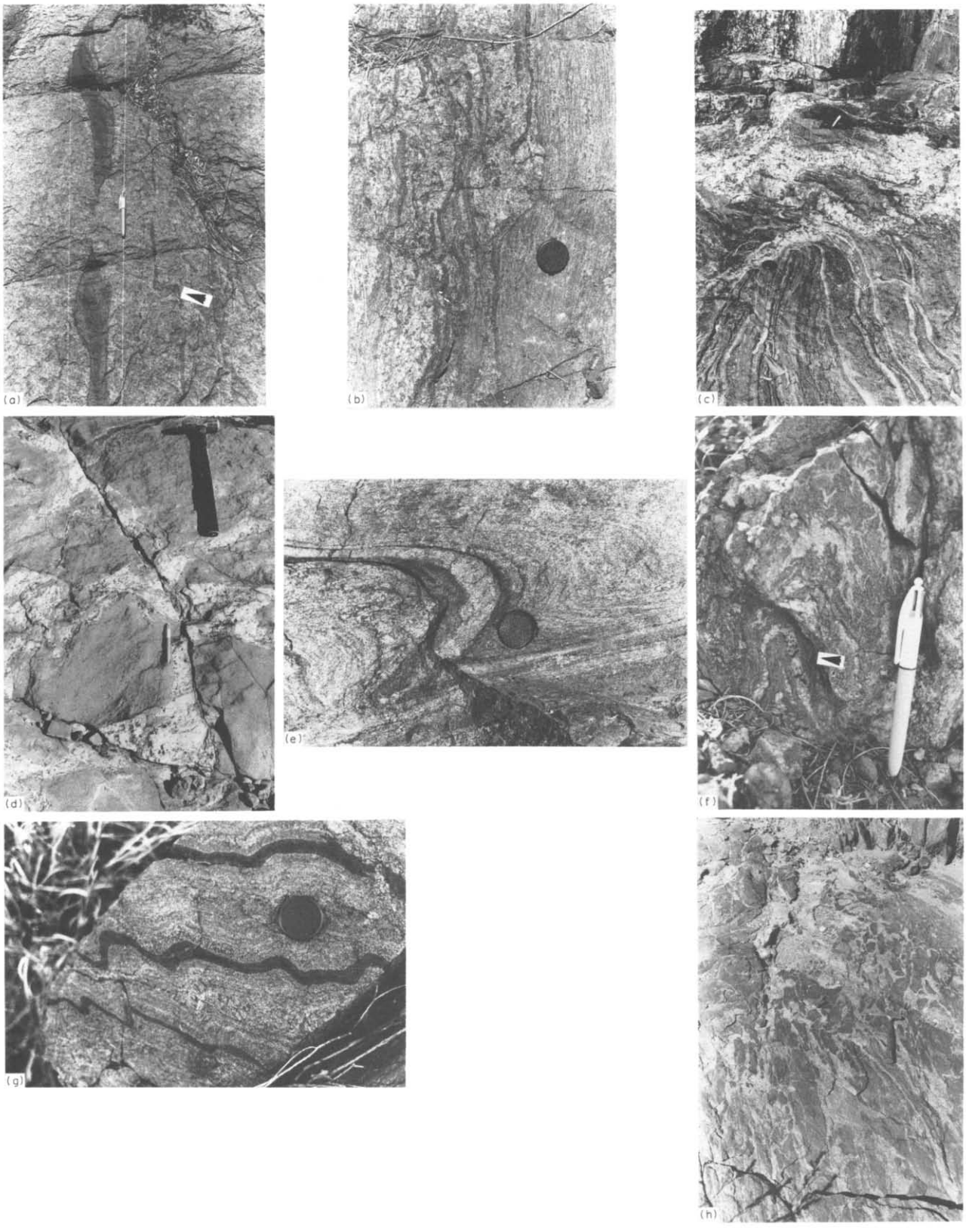

Fig. 2. (a) Asymmetric mafic granofels boudins and asymmetric F_2 fold (arrowed) in a felsic granofels with axial-planar S_{2a} quartz–feldspar leucosome: Ongeva Granulites. (b) Coarse (late D_2) S_{2b} sillimanite foliation cutting S_{2a} quartz–feldspar–biotite leucosome: Ongeva Granulites. (c) Irregularly-shaped, coarse-grained, pegmatitic pod of garnet + K-feldspar + quartz + biotite cutting S_{2b} sillimanite foliation and calc-silicate boudins: Ongeva Granulites. (d) Irregular pegmatitic network of plagioclase + hornblende cutting S_2 in mafic granofels: Ongeva Granulites. (e) Tight F_3 fold of S_{2a} leucocratic layering with axial-planar biotite and quartz elongation. Ongeva Granulites. (f) S_{2b} sillimanite foliation and D_2 cordierite–quartz leucosome (arrowed) tightly folded by F_3 with some sillimanite possibly axial planar. Anamarra Granite Domain. (g) Open asymmetric F_4 folds of S_{2a} quartz–feldspar leucosome and mafic granofels layers. Ongeva Granulites. (h) Amphibolite pod invaded by quartzofeldspathic gneiss in the Anamarra Granite Domain.

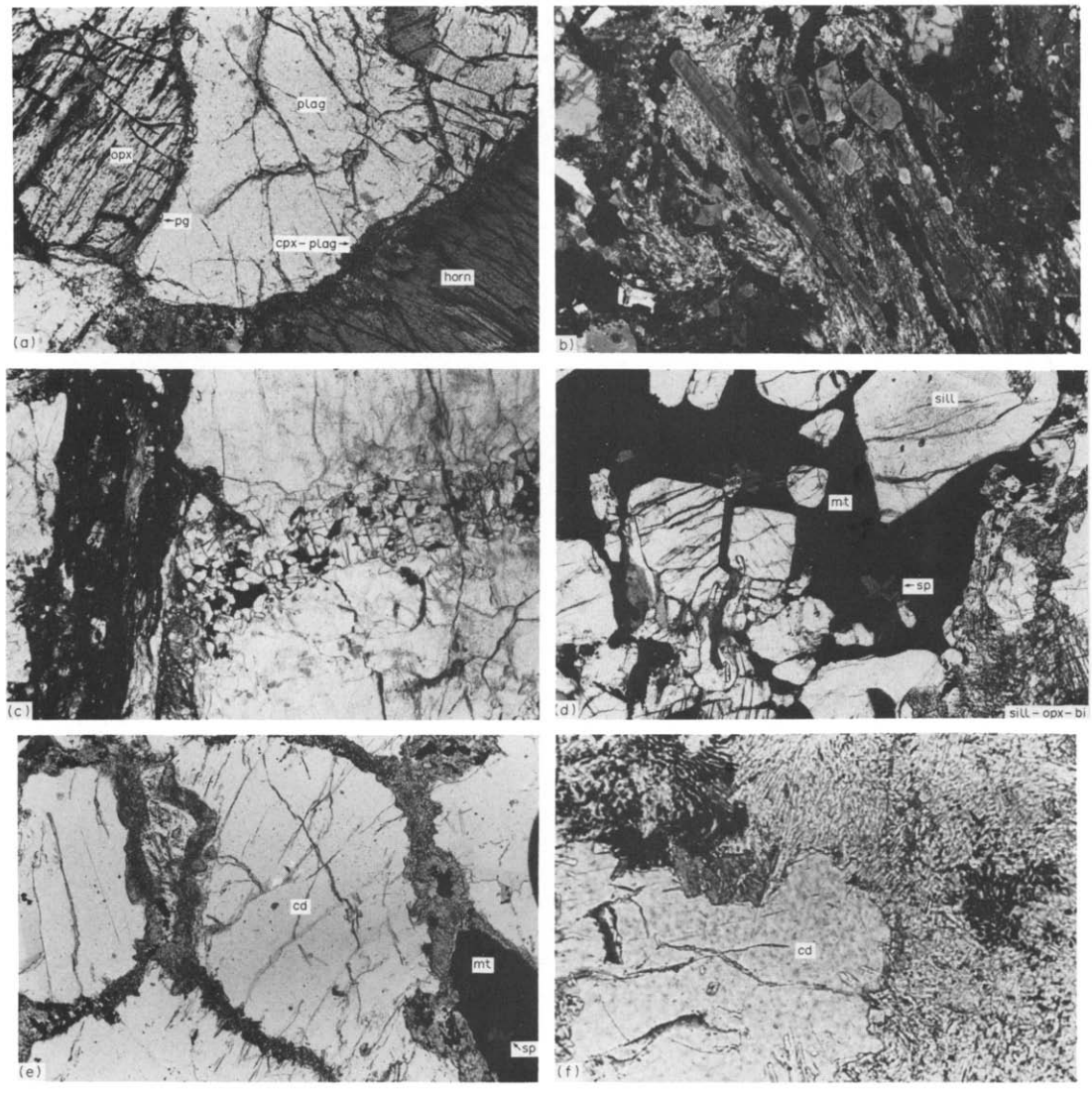

Fig. 3. (a) M_2 clinopyroxene + plagioclase corona at the interface of hornblende and plagioclase, and pargasite at the interface of orthopyroxene and plagioclase, in a mafic granofels from the Ongeva Granulites. Sample 375. Base of photograph is 1.75 mm. (b) S_{2b} sillimanite and magnetite isoclinally folded by F_3 in a cordierite gneiss from the Anamarra Granite Domain. Sample 372. Base of photograph is 4.4 mm (c) Coarse-grained S_{2b} sillimanite foliation truncated by a D_4 ultramylonite zone. Ongeva Granulites. Sample 377. Base of photograph is 12.0 mm (d) S_{2b} magnetite containing M_1 spinel inclusions. Note the coarse-grained S_{2b} sillimanite and the enveloping M_2 orthopyroxene + sillimanite + biotite symplectite. Ongeva Granulites. Sample 106. Base of photograph is 1.75 mm. (e) M_2 orthopyroxene + sillimanite + biotite + magnetite symplectite replacing cordierite along its grain boundaries. Symplectite encloses S_{2b} magnetite which has a M_1 spinel inclusion. Sample 257. Anamarra Granite Domain. Base of photograph is 4.4 mm. (f) Vermicular intergrowth of magnetite with M_2 orthopyroxene + sillimanite + biotite symplectite. Sample 702. Anamarra Granite Domain. Base of photograph is 0.7 mm.

Ongeva Granulites. A coarse-grained sillimanite + biotite foliation (S_{2b}) cuts the cordierite-bearing leucosome and both are folded by tight F_3 folds (Fig. 2f) and more open F_4 folds.

Two phyllonitic shear foliations enclose these high-grade blocks: (1) a steep NNE- to NE-trending retrograde shear foliation that contains a SE-trending biotite elongation lineation; and (2) an ESE-trending shear foliation with a NE-trending biotite, quartz or anthophyllite elongation lineation. The N-trending foliation indicates a poor NW-directed sense of shear, and bends into, and is truncated by, the E-trending shear foliation. The NNE-trending shear foliation has deformed felsic gneisses of granitic composition that commonly form irregular networks in the large meta-igneous amphibolitic pods (Fig. 2h). In places, the NNE-trending foliation is extensively crenulated by chevron folds. Crenulation pre-dated the E-trending shear fabric. The earlier shear foliation in the Anamarra Granite Domain may represent a late stage of the D_3 folding event in the Ongeva Granulites, as it pre-dates the E-trending shear foliations that appear to be continuous with the D_4 ultramylonite zones in the Ongeva Granulites.

The largest intrusion into the high-grade pods of paragneiss is a megacrystic granite, the Anamarra Granite of Shaw & Langworthy (1984). It contains a sub-horizontal NE-trending alignment of megacrysts, which is subparallel to the NE-trending shear foliation and which is cross-cut by narrow, discrete ESE-trending zones of mylonite. Deformation increases in intensity around the margin of the granite. The alignment of megacrysts in a foliation parallel to the regional NE-trending shear fabric (D_3?) may suggest that the granite crystallized during or prior to D_3. However, it is difficult to distinguish megacrystic foliations that formed by igneous flow from those that formed from regional deformation (cf. Paterson *et al.* 1989). Discrete E-trending (D_4) shear zones cutting the Anamarra Granite suggest that the granite had crystallized sufficiently by D_4 to accommodate inhomogeneous deformation.

In the northern part of the Anamarra Granite Domain, both the NNE- and E-trending shear foliations contain a stretching lineation that plunges to the NNE and both have sense of shear indicators recording north-side-up movement. This is probably due to re-activation of the foliations during the subsequent S-directed thrusting that resulted in the Gough Dam Schist Zone and shear zones transecting the Harts Range Group (D_5). Crenulation of biotite-schist interlayered with the E-trending shear foliation, further south, is probably a result of this subsequent thrusting. Similarly, coarse-grained quartz + K-feldspar + biotite + muscovite ± garnet pegmatites, veins of epidote and quartz, and meso-faults that cut the pervasive shear foliations in the Anamarra Granite Domain are probably related to fluid movement and deformation associated with the S-directed D_5 thrusting.

Harts Range Group

The Harts Range Group consists of interlayered, multiply-deformed amphibolites, metapelites, calc-silicates, quartzites and pods of mafic granulites, which are separated by E–W-trending, N-dipping mylonite zones that indicate a S-directed sense of shear. Deformation associated with mylonitization in the Harts Range Group post-dated the high-grade, penetrative deformation in the Strangways Metamorphic Complex (described below) and tight upright folding in the Harts Range Group. This thrusting will not be described in detail in this paper, even though there was probably some reworking of the Strangways Metamorphic Complex during shearing, evident as pods of mafic granulites amongst anastamosing S-directed ultramylonite zones north of the Gough Dam Schist Zone. (Fig. 1).

The last major folding episode of the Harts Range Group, prior to shearing, produced E–W-trending, tight to isoclinal, macroscopic folds with shallow plunges. The inferred shortening direction was along a NNE axis. We find no conclusive evidence to show that the Strangways Metamorphic Complex was a basement to the Harts Range Group, as inferred by Ding & James (1985), James & Ding (1988) and Oliver *et al.* (1988). Furthermore, the similar transport axes during folding of both the Harts Range Group and the Strangways Metamorphic Complex and stretching lineations in the mylonite zones may imply a related origin.

Gough Dam Schist Zone

The Gough Dam Schist Zone consists of well-foliated quartz + feldspar + biotite gneisses and biotite schists with a NNE-trending mineral-elongation lineation. Retrogressed chlorite and epidote foliations cut the biotite foliation. Within the gneiss, porphyroclasts and their recrystallized margins commonly have a symmetric shape with respect to the foliation. The asymmetry of porphyroclasts is usually indicative of non-coaxial deformation and can be used to determine a sense of shear (Simpson & Schmidt 1983). However, the lack of porphyroclast asymmetry in the Gough Dam Schist Zone probably suggests that non-coaxial deformation was not significant during the final stages of deformation. The gneissic foliation in the Gough Dam Schist Zone bounds some D_3 folds and cuts D_4 ultramylonites in the Strangways Metamorphic Complex, and may have resulted from flattening of a gneissic terrain around the granulites as a result of S-directed thrusting within the Harts Range Group during a D_5 deformation. Deformation in the Gough Dam Schist Zone was subsequent to the deformation and metamorphism in the discrete morphological units of the Strangways Metamorphic Complex that are discussed in this paper.

Geochronological constraints

On the basis of petrography and Rb–Sr data, Iyer *et al.* (1976) suggested that there were two distinct granulite-

facies metamorphisms: one at 1860 ± 80 Ma and another at 1470 ± 60 Ma. These probably correspond to our M_1 and M_2, since the corona and pseudomorphous textures described by Iyer *et al.* (1976) are similar to the textures that we describe below. Also, using Rb–Sr data, Black *et al.* (1983) inferred several events, but with a consistent early granulite-facies date of 1790 ± 35 Ma. Similarly, Allen & Stubbs (1982) inferred multiple recrystallization events from ^{40}Ar–^{39}Ar data, with a similar early granulite-facies event. Some gross disturbance to the Rb–Sr and ^{40}Ar–^{39}Ar isotopic systems of rocks in the Strangways Metamorphic Complex appear to have occurred in the period 1400–1000 Ma (Iyer *et al.* 1976, Allen & Stubbs 1982, Black *et al.* 1983) that may reflect limited uplift of the terrain (Warren 1983). Multiple deformations and metamorphisms have almost certainly disturbed the isotopic system of the rocks several times but it is almost impossible to be certain to what event the reported younger ages correspond. The problem is further compounded by the extensive, probably multiply worked, retrograde shear zones (D_5) that bound the Strangways Metamorphic Complex. However, much of the Rb–Sr and ^{40}Ar–^{39}Ar work is contradicted by U–Pb studies (Mortimer *et al.* 1987, Cooper *et al.* 1988), which suggest that shearing occurred around 1750 Ma and that no isotopic disturbances of the system occurred until ~500 Ma. All that we can be certain about is that the rocks were exposed when the Upper Proterozoic Heavitree Quartzite was deposited. The Alice Springs Orogeny in the mid-Carboniferous resulted in the further dislocation of the high-graded terrain, probably along re-activated shear zones (Stewart 1971, Collins & Tessyier 1989). Coarse-grained muscovite and chlorite ± epidote foliations overprint biotite foliations in the D_5 shear zones and may be associated with the later Palaeozoic event(s). The geochronological data are summarized in Table 1.

METAMORPHIC GEOLOGY

This section is primarily concerned with metapelitic rocks, because they are the most useful for inferring the metamorphic history in the Strangways Metamorphic Complex. However, metapelites are relatively uncommon in both the Ongeva Granulites and the Anamarra Granite Domain; so we also describe the enclosing calc-silicate, felsic and mafic gneisses. Much of the tectonometamorphic history is also contained in the shear zones that transect and bound the Strangways Metamorphic Complex; however, this will only be discussed briefly in this paper.

Felsic granofelses are interlayered with mafic granofelses in the Ongeva Granulites and in the eastern part of the Anamarra Granite Domain, and generally form layers greater than 10 m in thickness. Mafic granofelses outcrop predominantly in the Ongeva Granulites, forming about 50% of the outcrop. Mafic layers up to 10 cm thick occur in the felsic rocks and commonly form rootless, intrafolial, isoclinal folds; however, units up to 100 m in width also occur. Calc-silicates and marbles are not common, but occur interlayered with metapelitic gneisses. In some metapelites and mafic granofelses, calc-silicates form isolated boudins or impersistent layers of folded rock.

The rocks are interpreted to have been affected by two granulite-facies metamorphic events, M_{1-2}, and the relationship between the deformation events and these metamorphisms is summarized in Table 1. The mineral assemblages of mafic granulites indicate that metamorphic conditions reached granulite-facies grade (Turner 1968) during the early part of the tectonic history of the Strangways Metamorphic Complex (D_1) and probably remained at granulite-facies conditions during D_2. M_2 post-dated the S_{2b} sillimanite + biotite fabric and predated syn-F_4 pegmatite; therefore, it is probably related to D_3. D_4 ultramylonitization was probably at or near granulite-facies conditions (Norman 1989) and post-dated M_2. Near E-trending zones in the Anamarra Granite Domain, and on the northern margin of the Ongeva Granulites, calc-silicate gneisses have been extensively retrogressed to epidote-rich assemblages. This later retrogression is probably related to subsequent southward thrusting along shear zones.

PETROGRAPHY

Felsic granofels

The felsic gneisses vary from equigranular, medium-grained, granoblastic, quartz-rich, K-feldspar + plagioclase + orthopyroxene gneisses and granofels to garnet-bearing, K-feldspar + quartz + biotite migmatites. The proportion of plagioclase varies considerably. The S_{2a} foliation is mainly defined by deformed, coarse-grained leucocratic layers and the alignment of some biotite grains, although biotite may have largely crystallized during the development of the later S_{2b} foliation. The S_{2a} foliation contains boudinaged, large, subrounded K-feldspar grains, most probably remnants from D_1. These large K-feldspar grains are contained in medium-grained, granoblastic leucocratic layers, which presumably crystallized from melt during D_2. Deformation features in S_{2a} leucocratic layers include: extensively recrystallized quartz grains, which show well-defined dentate grain boundaries; small subgrains and minor myrmekite around the margins of K-feldspar; plagioclase grains with deformation twins and minor recrystallization. These features post-date M_1 and S_{2a} assemblages and may be related to deformation late in D_2 or later recrystallization associated with D_3. Orthopyroxene is invariably rimmed by grey–blue pargasitic hornblende. Pargasitic hornblende and fine-grained biotite after orthopyroxene, together with a quartz mylonitic fabric form an axial-planar foliation (S_3) to tight, intrafolial F_3 folds indicating that hydrous, mylonitic conditions existed early in D_3. The quartz stretching lineations contained in S_3 are parallel to the fold axes. Garnet is generally poikioblastic, with inclusions of

quartz and K-feldspar, and has small biotite grains along micro-cracks and around its margins. Large, brown S_{2b} biotite grains which are generally sub-parallel to S_{2a} leucocratic layers, are commonly kinked owing to post-D_2 deformation.

Mafic granofels

A high-grade gneissic layering (S_2) is defined by alternating, medium-grained, hornblende + orthopyroxene-rich and plagioclase-rich layers. Thin plagioclase layers may contain subidioblastic, coarse-grained orthopyroxene or coarse-grained hornblende aligned in this S_2 foliation. The mesosomes have a granoblastic texture consisting of orthopyroxene, clinopyroxene, green–brown hornblende, plagioclase and magnetite. Hornblende may form up to 70% of the mafic layers. The S_2 layering is sub-parallel to the gross compositional layering (S_1) and axial planar to F_2 folds. A fine-grained, granoblastic, two-pyroxene S_1 layering is folded by F_2. Granulite-facies conditions, as evidenced by the two-pyroxene assemblages, existed at peak metamorphism (M_1–D_1) and persisted during D_2. The main, penetrative S_2 foliation is cut by irregular networks of coarse-grained orthopyroxene–plagioclaserock that may contain a weak foliation parallel to S_2. These coarse-grained networks may be coeval with the garnet-bearing pegmatite pods in metapelites and orthopyroxene-bearing pods in felsic granofels; they appear to have crystallized from melt early in D_3 or late in D_2. Orthopyoxene in these late melts is invariably rimmed by grey–blue pargasite.

S_2 hornblende grains have coronas of granular, subidioblastic clinopyroxene and plagioclase where in contact with plagioclase grains (Fig. 3a). Clinopyroxene in the S_2 foliation is usually recrystallized around its margins and orthopyroxene is rimmed by pargasite (Fig. 3a). These corona and recrystallization textures are cut by D_4 ultramylonites and are inferred to be the effects of M_2.

Metapelites

Metapelites, which have a rust-red outcrop colour, are characterized by abundant sillimanite, garnet and biotite, and commonly grade into quartz + feldspar + biotite migmatites. The most obvious foliation in these rocks consists of poorly-lineated, coarse-grained sillimanite, large biotite grains and magnetite (S_{2b}). Medium- to coarse-grained K-feldspar + quartz ± biotite leucocratic layers, which delineate the main S_{2a} foliation, are cut by this coarse-grained sillimanite S_{2b} foliation (Fig. 2b). Corundum is a minor mineral occurring with sillimanite, but isolated from quartz and feldspar by either biotite or sillimanite. We interpret this foliation as having formed late in D_2, due to a flattening strain. The coarse-grained sillimanite–magnetite foliation is tightly folded by F_3 folds (Fig. 3b) and is cut by D_4 ultramylonite zones (Fig. 3c). Garnet occurs as large, irrregular, elongate, poikioblastic or idioblastic grains that define the early S_{2a} foliation, but may also overprint the coarse-grained sillimanite foliation. Garnet appears to have been present at M_1 and throughout D_2. Garnet that is elongate in the S_{2a} foliation may contain folded inclusions of fine-grained sillimanite suggesting that sillimanite was part of the S_1 assemblage and that S_{2a} is a tectonic fabric.

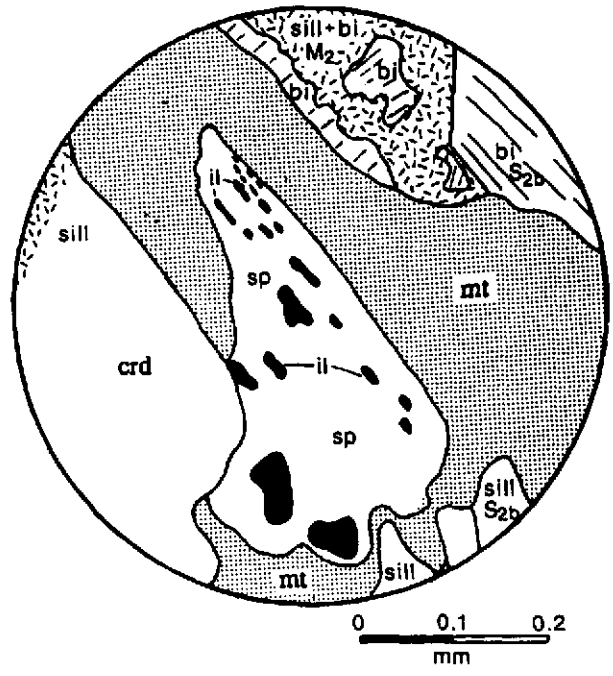

Fig. 4. Diagram of a S_{2b} magnetite containing a M_1 spinel inclusion which has inclusions of ilmenite. Sample 709. Anamarra Granite Domain.

Coarse-grained magnetite occurring with S_2 sillimanite invariably contains subidioblastic inclusions of spinel (Fig. 3d), which may contain idioblastic inclusions of ilmenite (Fig. 4). Spinel also occurs as inclusions in sillimanite and garnet. Coronas of S_2 sillimanite around spinel are also observed in garnet quartz–feldspar gneisses. Spinel and ilmenite are inferred to have formed part of the peak assemblage, with coarse-grained sillimanite, magnetite and biotite developed during retrogression.

In the metapelites of the Anamarra Granite Domain, spinel also occurs as inclusions in medium-grained granoblastic cordierite that is enveloped and cut by coarse-grained S_{2b} sillimanite, biotite and magnetite. Small sillimanite needles are contained in some garnet grains, forming inclusion trails that are folded (F_2) or at a high angle to the enveloping and cross-cutting S_{2b} sillimanite foliation. Hence, cordierite is interpreted as having been present with spinel, ilmenite, K-feldspar, garnet, sillimanite and quartz at peak metamorphic conditions (M_1). As in the felsic granofelses, quartz has undulose extinction and is extensively recrystallized, feldspar has subgrains along the grain boundaries, and large S_{2b} biotite grains are kinked.

In the Anamarra Domain metapelites, cordierite has been replaced along its grain boundaries and cleavage planes by poorly-oriented, fine-grained symplectic aggregates of orthopyroxene + sillimanite + biotite + magnetite (Fig. 3e). In the Ongeva Granulites, the

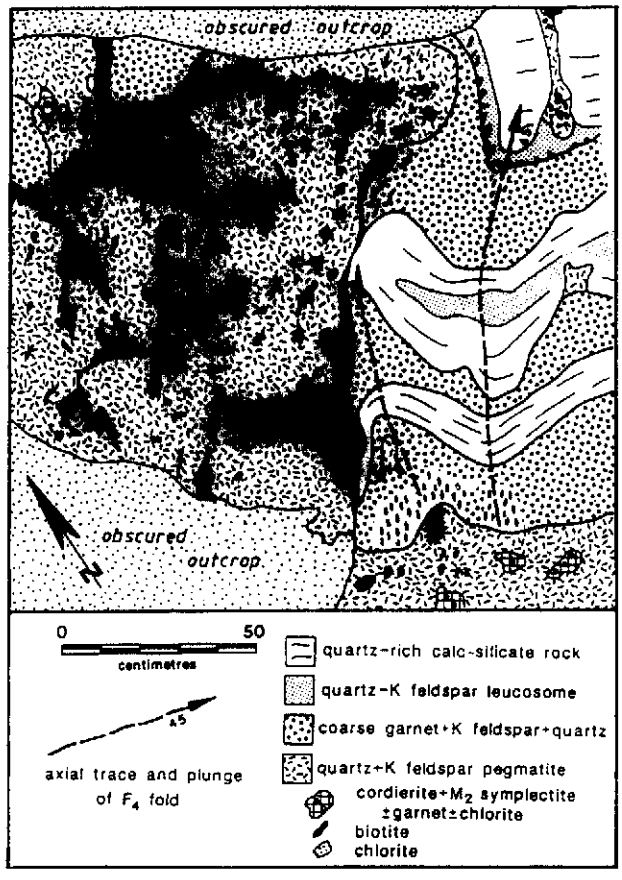

Fig. 5. Outcrop sketch of open F_4 folds and late D_3 quartz–feldspar–biotite pegmatite containing xenoliths of cordierite with M_2 symplectic aggregates.

orthopyroxene + sillimanite + biotite + magnetite symplectite commonly totally pseudomorphs cordierite. The sillimanite is random, the orthopyroxene (av. $X_{mg} = 58.1$, av. wt% $Al_2O_3 = 6.49$, Table 2) is unaltered, and magnetite forms a vermicular intergrowth (Fig. 3f). Aluminous orthopyroxene may be expected to occur at high temperatures, in the presence of garnet (Harley 1984); however, it is more probable that, in places, the high Al content of orthopyroxene reflects excess alumina from the breakdown of cordierite not involving the matrix garnet, quartz and feldspar. Sapphirine occurring with some symplectites (see below) supports this interpretation. Vermicular magnetite also occurs around the margins of garnet grains. Coarse-grained S_{2b} sillimanite has 'beards' of fine-grained sillimanite and may be enclosed by the symplectite. The symplectic aggregates are fine-grained and quite distinct from the coarse-grained S_2 minerals, but are cut by the D_4 ultramylonite zones. Coexisting orthopyroxene and sillimanite imply higher pressure conditions than any of the mineral assemblages observed for S_{1-2} (see below). From this and their textural distinction, we designate the metamorphic event responsible for this symplectite as M_2. M_2 symplectite after cordierite has been found in cm-size cordierite xenoliths inclusions within a quartz + K-feldspar + biotite pegmatite that crystallized during F_4 (Fig. 5), since biotite in this pegmatite is aligned in the axial plane of open F_4 folds. The 'country rock' consists of similar cordierite gneiss containing the M_2 assemblage. From this evidence, M_2 occurred before F_4 folding and D_4 ultramylonitization but obviously after S_{2b}. Therefore, the pressure increase indicated by M_2 assemblages was probably a response to D_3. That the rocks were not entirely recrystallized during this event presumably reflects a lower water activity than at peak metamorphism, inhibiting recrystallization.

Quartz-free assemblages

Silica-undersaturated rocks have not been observed in the area. However, quartz-free assemblages containing sapphirine, corundum and spinel exist on a microscopic scale. As mentioned above, primary spinel is preserved in retrograde magnetite and sillimanite, and in D_{1-2} garnet and cordierite. Corundum occurs within biotite and sillimanite S_{2b} folia; quartz and feldspar are absent from these areas in the rock. Sapphirine occurs as small idioblastic to subidioblastic grains with sillimanite, orthopyroxene and biotite in the M_2 symplectites contained in the metapelitic gneisses. Primary sapphirine as inclusions within cordierite has not been observed.

Calc-silicate rocks

Calc-cilicate rocks preserve a high-grade S_2 gneissosity defined by alternations in the proportion of quartz-rich layers and scapolite ($X_{mei} = 80.6$) + wollastonite + diopside + anorthite + grossular rich layers. This layering is parallel to the regional compositional layering (S_1). S_2 is medium-grained and granoblastic. Other minor minerals in S_2 include calcite, quartz, sphene and magnetite. Scapolite invariably is recrystallized on grain margins, and both diopside and plagioclase have coronas of garnet. In wollastonite-rich rocks scapolite also has a corona of garnet and the wollastonite occurs as large xenoblastic grains lacking a corona. Diopside shows undulose extinction, and quartz-rich layers show extensive recrystallization. The garnet coronas are post metamorphic peak and may be related to cooling during D_2 or to M_2. Rare calcite-rich rocks may occur interlayered with the calc-silicates. These marbles are medium-grained and contain diopside, scapolite, garnet, spinel and phlogopite.

Ultramylonites

The D_4 ultramylonites that transect the D_3 structures are of variable composition and show neocrystallization of sillimanite and biotite and recrystallization of orthopyroxene, clinopyroxene, garnet and hornblende. Myrmekite is common adjacent to the shear zones and was probably induced by strain and fluid movement (Ashworth 1972). A marble breccia caught between ultramylonite zones and inferred to have been ductile during D_4 ultramylonitization contains folded fragments of ultramylonite, recrystallized calcite and inclusions within the calcite of scapolite and K-feldspar with garnet coronas (Norman 1989). This suggests that the corona textures in

the calc-silicate rocks developed prior to D_4 ultramylonitization.

Summary

In the Ongeva Granulites, M_1 is characterized by a two pyroxene–hornblende–plagioclase assemblage in mafic rocks, quartz + K-feldspar + orthopyroxene in felsic rocks, and wollastonite + scapolite + diopside + anorthite in calc-silicate rocks. A primary assemblage in metapelites of the Ongeva Granulites is difficult to recognize because of overprinting reactions that occurred during D_2–D_4. Overprinting of metapelitic assemblages was not as severe in the Anamarra Granite Domain, and a probable primary M_1 assemblage is cordierite + sillimanite + garnet + spinel + ilmenite + quartz + K-feldspar. Anatexis was probably associated with peak metamorphism with melt crystallizing into leucocratic layers during D_2 in a ductile, non-coaxial regime and crystallizing into irregular pegmatitic pods late in D_2 and early in D_3. The formation of sillimanite + biotite + magnetite-bearing S_{2b} assemblages in metapelites, towards the end of D_2, involved the hydration and retrogression of peak M_1 assemblages. Possible sources of hydrous fluids may be from crystallizing melt or from the intrusion of granite in the Anamarra Granite Domain.

The effects of a second metamorphic event, M_2, are restricted to either the pseudomorphing of, or the reaction to high-grade, anhydrous coronas around M_1 minerals. Symplectic intergrowths of orthopyroxene + sillimanite + biotite + magnetite pseudomorphed cordierite in metapelitic gneisses, fine-grained clinopyroxene + plagioclase coronas around hornblende developed in mafic gneisses, and pargasitic hornblende formed around the margins of orthopyroxene in mafic and felsic granulites. In calc-silicate rocks, garnet coronas around diopside, plagioclase and scapolite may also be the result of M_2. M_2 textures are cut by the D_4 ultramylonite zones. M_2 was a response to D_3 folding in the Ongeva Granulites and possibly the development of the NE-trending shear fabric in the Anamarra Granite Domain.

Neocrystallization of sillimanite in D_4 ultramylonites suggests that conditions were hot (Norman 1989), and the persistence of orthopyroxene in the ultramylonites suggests that water activity was fairly low (c.f. Sandiford 1985a) during D_4. Granulite-facies conditions probably existed during D_4.

A petrogenetic grid to account for the mineral assemblages

Characteristic mineral parageneses have been identified for different stages in the metamorphic and deformation history of the Strangways Metamorphic Complex. The relative P–T conditions of these mineral assemblages can be established using petrogenetic grids involving all the observed minerals (e.g. Hensen 1971) and can be used to infer a P–T path followed by the rocks during their evolution. The inclusion of spinel, ilmenite and magnetite in the inferred mineral assemblages requires a consideration of the model system, K_2O–FeO–MgO–Al_2O_3–SiO_2–H_2O (KFMASH) augmented by the addition of Fe_2O_3 and TiO_2 (KFMASHTO). The extension of a KFMASH petrogenetic grid, which is applicable to granulite-facies conditions, into KFMASHTO was presented by Clarke *et al.* (1989). This KFMASHTO grid has been used successfully to explain metamorphic assemblages and corona reaction textures in spinel + quartz-bearing rocks metamorphosed under similar conditions to the rocks comprising the Strangways Metamorphic Complex (Clarke *et al.* 1989, 1990, Stüwe & Powell 1989a,b). Sillimanite was present as part of the primary (M_1) assemblage and was involved in all the overprinting mineral assemblages in the metapelites described above, so the petrogenetic grid can be simplified by projecting from sillimanite (Fig. 6). The location of the inferred metamorphic peak, S_2 and M_2 assemblages are indicated in Fig. 6 by shading.

All the metapelites from the Anamarra Granite Domain contain coarse-grained garnet, quartz, K-feldspar and cordierite, suggesting that they were part of the primary M_1 mineral assemblage. Remnants of spinel and ilmenite occur as inclusions in magnetite and garnet, suggesting that spinel and ilmenite were also present at peak conditions. Ilmenite is rare, and occurs only as inclusions; it is never in textural equilibrium with quartz and feldspar. Spinel is comparatively abundant, occurring as inclusions in magnetite, garnet, sillimanite and cordierite. The pervasive, coarse-grained S_{2b} sillimanite + biotite + magnetite foliation cuts through all these minerals.These textures are best explained by the rocks cooling through and reacting across reactions A and B in Fig. 6. They imply an approximately isobaric cooling path during D_2, but any change in pressure is poorly constrained. However, isobaric cooling or limited compression with cooling is implied by the absence of cordierite overgrowths on garnet, or garnet overgrowths on cordierite, which appear to be formed readily with even minor compression (Stüwe & Powell 1989a) or marked compression (Stüwe & Powell 1989b), respectively.

In the Ongeva Granulites, the late fine-grained orthopyroxene + sillimanite + biotite + magnetite symplectic aggregates pseudomorph a coarse-grained mineral that was part of the peak assemblage. In places, remnant cores of cordierite are preserved. In the Anamarra Granite Domain this simplectic aggregate rims cordierite. The textures and inferred primary assemblages in metapelites are consistent between the two domains; the degree of late overprinting simply being greater in the Ongeva Granulites in the eastern part of the area.

The pseudomorphous, fine-grained, orthopyroxene + sillimanite + biotite + magnetite symplectic aggregates are quite distinct from the coarse-grained S_{2b} sillimanite + biotite + magnetite foliation. The petrogenetic grid (Fig. 6) implies that conditions were at some considerably higher pressure during crystallization of the symplectite (M_2) than during crystallization of either the peak (M_1) assemblage or the S_{2b} mineral assem-

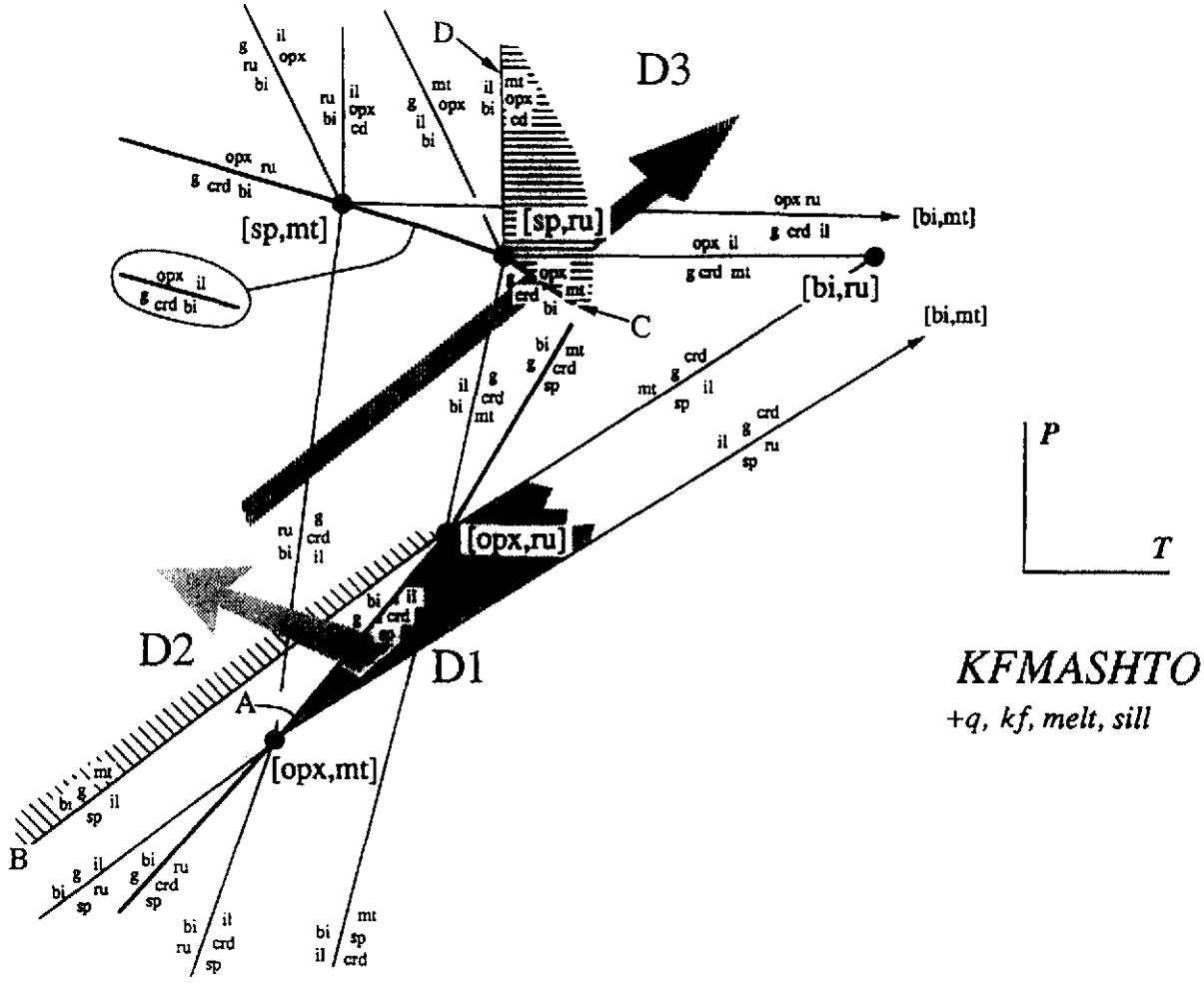

Fig. 6. K_2O–FeO–MgO–Al_2O_3–SiO_2–MgO–H_2O–TiO_2–O_2 (KFMASHTO) petrogenetic grid, for a projection from quartz, K-feldspar, sillimanite and melt, after Clarke *et al.* (1989). The shaded areas represent the metamorphic conditions implied by the peak (S_1), S_2 and M_2 (D_3) assemblages described in the text. The reactions marked as A, B, C and D are the reactions that are inferred to be involved in the development of the overprinting mineral assemblages. The large arrows show the inferred *P–T* path for the Strangways Metamorphic Complex: after approximately isobaric cooling from peak M_1 conditions, the terrain experienced an increase in pressure during the M_2–D_3 event. See Table 1 for the correlation between metamorphic and deformation events.

blages; that is M_2 was at a greater pressure than reaction C and probably at a greater temperature than reaction D (Fig. 6). Cordierite was partly or wholly consumed in the development of the M_2 assemblage. It seems inescapable that the terrain has suffered a late increase in pressure after the development of the S_{2b} foliation. Field evidence (Fig. 5) constrains this increase in pressure to occur sometime during D_3. The grid also suggests that the rocks experienced comparable, or slightly higher temperature conditions during this event than at the end of D_2 when the coarse-grained sillimanite foliation formed (Fig. 6).

Corundum occurs in the coarse-grained S_{2b} sillimanite foliation and, less commonly, idioblastic sapphirine occurs with the M_2 sillimanite + orthopyroxene symplectite. Corundum and sapphirine are never in contact with quartz and feldspar in the S_{2a} foliation; they are presumably the product of some local equilibrium, on a scale less than the width of the S_{2b} foliation or the diameter of the grains that the symplectites pseudomorphed.

Quantitative pressure estimates for M_1 *and* M_2

The mineral assemblages in metapelites described in the previous sections have potential for the estimation of conditions using the "average pressure approach" of Powell & Holland (1988), with the expanded internally consistent thermodynamic dataset of Holland & Powell (1990). Mineral analyses were obtained at Macquarie University using an ETEC electron microprobe with an accelerating voltage of 15 kV. Representative analyses of metapelitic assemblages are presented in Table 2. The application of the average-pressure approach to these and similar metapelites (e.g. Clarke *et al.* 1990), is complicated by the problem of re-equilibration during cooling, affecting mineral compositions by, for example, Fe–Mg exchange, even if the primary assemblage can be satisfactorily identified. Of course, the problem is compounded by the partial recrystallization of the metapelites during D_2 and D_3. These problems are particularly acute with respect to spinel, because extensive exsolution of magnetite has occurred during the development

of S_2. Moreover, if biotite is to be effectively included in the calculations, the activity of H_2O is an extra variable. In the rocks considered here, that were partially melted at the metamorphic peak, a (H_2O) was less or much less than unity.

As a consequence of these potential difficulties, the most successful calculations were obtained on S_2 assemblages, these minerals defining the main penetrative foliation (Table 2). Using all S_2 mineral end-members in sample 704, gave $P = 5.4 \pm 0.9$ kbar (all $\pm$ at 2σ) at

Table 2. Representative microprobe analyses of mineral assemblages in samples 704, 257 and 702 used in average-pressure calculations

Representative microprobe analyses of minerals in sample 704

wt%	sp	il	crd	kf	g (core)	g (rim)	sill (S_{2b})	bi (S_{2b})	opx (M_2)	sil (M_2)
SiO_2	—	0.09	49.7	64.92	39.05	38.91	37.3	37.2	49.05	39.43
TiO_2	—	51.49	—	—	—	—	—	3.09	—	—
Al_2O_3	59.79	0.19	33.36	18.71	22.02	22.42	62.39	15.57	6.42	52.93
Cr_2O_3	0.34	—	—	—	—	—	—	0.08	—	—
FeO	27.53	42.12	3.7	—	30.23	30.69	0.97	15.14	23.93	4.01
MnO	0.09	3.74	—	—	0.42	0.61	—	—	0.44	—
MgO	8.12	0.36	11.23	—	8.52	8.96	—	14.82	19.87	2.88
CaO	—	—	—	0.1	1.29	0.26	—	0.05	0.11	—
Na_2O	0.04	—	0.19	2.08	—	0.26	—	0.46	—	—
K_2O	—	—	—	13.59	—	—	0.04	9.53	—	—
ZnO	5.17	—	—	—	—	—	—	0.08	—	—
Total	101.08	97.99	98.18	99.4	101.53	101.85	100.7	96.02	99.82	99.25

Structural analysis of minerals in sample 704

	4(O)	3(O)	18(O)	32(O)	24(O)	24(O)	5(O)	22(O)	6(O)	5(O)
Si	—	0.002	5.015	11.959	5.979	5.938	37.300	5.528	1.844	1.095
Ti	—	0.994	—	—	—	—	—	0.345	—	—
Al	1.940	0.006	3.963	4.058	3.969	4.028	62.390	2.723	0.284	1.730
Cr	0.007	—	—	—	—	—	—	0.010	—	—
Fe	0.634	0.904	0.312	—	3.871	3.917	0.970	1.882	0.753	0.093
Mn	0.002	0.081	—	—	0.055	0.079	—	—	0.014	—
Mg	0.334	0.014	1.690	—	1.945	2.039	—	3.283	1.114	0.119
Ca	—	—	—	0.020	0.211	0.043	—	0.008	0.005	—
Na	0.002	—	0.037	0.742	—	—	—	0.133	—	—
K	—	—	—	3.194	—	—	0.040	1.807	—	—
Zn	0.105	—	—	—	—	—	—	0.009	—	—
Total	3.024	2.001	11.016	19.974	16.030	16.044	100.710	15.727	4.013	3.037
XMg	34.5	1.5	84.4	—	33.4	34.2	—	63.6	59.7	56.1

Representative microprobe analyses of minerals in sample 257

wt%	sp	crd	kf	g (core)	g (rim)	sill (S_{2b})	bi (S_{2b})
SiO_2	—	49.38	65.56	37.58	36.23	37.29	36.84
TiO_2	—	—	—	—	—	—	3.61
Al_2O_3	61.3	33.8	18.75	23.03	23.54	61.67	17.12
Cr_2O_3	0.35	—	—	—	—	—	—
FeO	26.55	5.07	—	32.06	32.21	1.16	15.65
MnO	0.59	0.28	—	1.11	1.08	—	0.12
MgO	7.98	10.39	—	7.9	8.17	—	14.04
CaO	—	—	0.14	0.13	0.18	—	—
Na_2O	0.08	0.13	2.22	—	—	—	0.26
K_2O	—	—	13.06	—	—	—	8.73
ZnO	6.04	—	—	—	—	—	—
Total	102.89	99.05	99.73	101.8	101.41	100.12	96.37

Structural analysis of minerals in sample 257

	32(O)	18(O)	32(O)	24(O)	24(O)	5(O)	22(O)
Si	—	4.977	11.995	5.798	5.635	1.010	5.428
Ti	—	—	—	—	—	—	0.400
Al	15.614	4.011	4.040	4.183	4.311	1.9767	2.970
Cr	0.061	—	—	—	—	—	—
Fe	4.803	0.427	—	4.137	4.189	0.026	1.929
Mn	0.108	0.024	—	0.145	0.142	—	0.015
Mg	2.573	1.561	—	1.818	1.895	—	3.084
Ca	—	—	0.027	0.022	0.030	—	—
Na	0.330	0.026	0.788	—	—	—	0.074
K	—	—	3.048	—	—	—	1.641
Zn	0.965	—	—	—	—	—	—
Total	24.156	11.025	19.897	16.104	16.203	3.003	15.540
XMg	34.9	78.5	—	30.5	31.1	—	61.5

Table 2 (*continued*)

Representative microprobe analyses of cordierite and M_2 symplectite in sample 702							
wt%	crd	crd	opx (M_2)	opx (M_2)	sill (M_2)	sill (M_2)	bi (M_2)
SiO_2	49.55	50.64	49.36	49.64	38.09	38.6	38.48
TiO_2	—	—	—	—	—	—	3.34
Al_2O_3	33.58	34.17	6.61	6.36	59.29	60.46	16.76
FeO	5.63	3.95	25.41	24.64	2.7	2.36	14.9
MnO	—	0.12	0.5	0.46	—	—	—
MgO	10.18	11.47	19.09	19.75	1.32	0.96	15.24
Na_2O	0.09	0.09	—	—	—	—	0.23
K_2O	0.07	—	—	—	—	—	9.04
Total	99.1	100.44	100.97	100.85	101.4	102.38	97.99
Structural analysis of minerals in sample 702							
	18(O)	18(O)	6(O)	6(O)	5(O)	5(O)	22(O)
Si	4.998	5.001	1.845	1.850	1.028	1.029	5.541
Ti	—	—	—	—	—	—	0.362
Al	3.987	3.973	0.291	0.279	1.884	1.898	2.841
Fe	0.475	0.327	0.794	0.768	0.061	0.053	1.794
Mn	—	0.010	0.016	0.015	—	—	—
Mg	1.530	1.689	1.064	1.098	0.053	0.038	3.273
Na	0.017	0.017	—	—	—	—	0.063
K	0.009	—	—	—	—	—	1.661
Total	11.016	11.016	4.009	4.010	3.027	3.019	15.534
XMg	76.3	83.8	57.3	58.8	46.6	42.2	64.6

750°C and a (H_2O) = 0.3, but the calculation may be improved by excluding eastonite (on the basis of the diagnostics, Powell & Holland 1988), to arrive at $P = 5.1 \pm 1.0$ kbar with σfit = 1.3. Excluding eastonite from the calculations, the effect of a (H_2O) can be considered: there is a moderate dependence for this assemblage, with average pressure decreasing with decreasing a (H_2O) (Table 3). However, all calculations are within statistical error of each other, and σfit is minimized for low a (H_2O) (Table 3), consistent with the rocks being at granulite facies. A temperature of 750°C is used in this section because, although the calculations turn out to be weakly dependent on temperature (e.g. Table 3), this is the preferred temperature of similar spinel-bearing mineral assemblages elsewhere (Stüwe & Powell, 1989a,b). Calculations on the S_2 assemblages in sample 257 gave a similar result of $P = 6.0 \pm 0.70$ kbar for 750°C and a (H_2O) = 0.3. Eastonite was excluded on the basis of diagnostics (Table 3). Hence, D_2 in the Strangways Metamorphic Complex is inferred to occur at pressures between 4 and 6 kbar, consistent with calculations on similar spinel-bearing assemblages from elsewhere (Stüwe & Powell, 1989a,b). From arguments presented in the previous section, peak metamorphic conditions probably occurred at higher temperatures than D_2 assemblages but at similar pressures. Scapolite ($X_{mei} = 80.6$) + wollastonite + grossular + anorthite assemblages in calc-silicate rocks infer a high temperature at peak metamorphism of about 800–850°C, slightly higher than that for D_2 assemblages. Hercynitic spinel + quartz assemblages at peak metamorphism would infer low pressures at these temperatures, based on experiments by Richardson (1968), consistent with the average-pressure calculations. Using the stability data of Hensen & Green (1973) for cordierite and garnet (CAGS geobarometer), an upper pressure of 6 kbar is obtained for D_2 confirming the average-pressure calculations. The calculated pressures are significantly lower than initial pressures of 8 ± 1 kbar inferred by Warren (1982, 1983) for the Strangways Metamorphic Complex. Oliver *et al.* (1988) have also inferred lower initial pressures than Warren (1982, 1983) but did not recognize any subsequent increase in pressure.

A successful calculation for the conditions of M_2 was obtained on the pseudomorphous, symplectic sillimanite–orthopyroxene aggregate in sample 702 (Table 3), giving $P = 7.5 \pm 0.8$ kbar at 800°C and a (H_2O) = 0.5, and σfit = 1.5 when eastonite was excluded on the basis of the diagnostics. Excluding eastonite, the average pressure calculations show only a weak dependence on a (H_2O) (Table 3) but with σfit minimized for a (H_2O) = 0.5. Omitting eastonite from the calculations, the effect of temperature may be considered: average pressures increasing with increasing temperature, but with σfit minimized for a temperature of 800°C (Table 3).

In conclusion, the average-pressure calculations are consistent with D_2 occurring at 5.5 ± 0.8 kbar and at temperatures of 750°C. Calc-silicate assemblages suggest that peak metamorphic temperatures of about 800–850°C. The texturally-distinct, post-S_2 sillimanite + orthopyroxene symplectites imply conditions for M_2 of 7.5 ± 0.8 kbar and 800°C. That the D_3 assemblage occurs at higher temperatures than implied by the S_2 assemblages is consistent with the topology of the petrogenetic grid (Fig. 6). However, higher temperature conditions did not erase evidence of the S_2 assemblage. Presumably there was an insufficient influx of water during D_3 to enable M_2 to establish the dominant mineral assemblage in the Strangways Metamorphic

Complex. The quantitative estimates of metamorphic conditions confirm the *P–T* path qualitatively outlined by the crossing of univariant reactions on the petrogenetic grid.

DISCUSSION

A P–T–t *path for the Strangways Metamorphic Complex*

The *P–T* path outlined above for the Strangways Metamorphic Complex is complimentary to the work of Warren (1982, 1983), as summarized in Table 1. However, we recognize an early low-pressure metamorphism, here called M_1, characterized by spinel + quartz-bearing assemblages in metapelites. Isobaric cooling from peak M_1 conditions occurred at $P = 5.5 \pm 0.8$ kbar, during compression that produced the main penetrative foliations in the terrain, S_1 and S_2. From assemblages in Division 1, metapelitic rocks in the Reynolds Range, 150 km northwest of the Strangways Range, Warren & Stewart (1988) also inferred lower initial pressures (<6kbar) as part of an anticlockwise *P–T–t* path. The ~1800 Ma Rb–Sr age of Black *et al.* (1983) that they related to a granulite-facies metamorphism called the "Strangways Event" and the early granulite-facies "Arunta Orogeny" of Allen & Stubbs (1982), are most probably related to our M_1 event. An initial stage of cooling was referred to by Warren (1982, 1983) as the "biotite stage", and probably corresponds to the cooling from D_1 to D_2 described herein, during which the coarse-grained sillimanite S_{2b} foliae formed. There is some overlap of the granulite and biotite stages of Warren (1983) because of our interpretation of cooling during D_2 from M_1, at granulite-facies conditions (see Table 1).

Table 3. Average-pressure calculations on the mineral parageneses in samples 704, 257 and 702 following the approach of Powell & Holland (1988) with the expanded internally consistent dataset of Holland & Powell (1990)

S_2 assemblage in sample 704: g–bi–crd–sp–sill

End members	phl	ann	east	naph	crd	fcrd	py	alm	ab	kf	sp	herc	q	sill
Activities (a)	0.156	0.012	0.032	0.031	0.636	0.034	0.033	0.255	0.563	0.789	0.34	0.65	1.0	1.0
σ (ln a)	0.220	0.534	0.406	0.324	0.040	0.399	0.415	0.121	0.057	0.013	0.131	0.037	0	0

Independent reactions	Calculated pressures at T = 750°C and a (H_2O) = 0.3 $P(T)$	σ	dT/dP	ln K
(1) py + 2sill = crd + sp	4.9	0.68	0.0023	1.877
(2) 3alm + 6sill = 2fcrd + 5herc + 5q	5.7	0.62	0.0107	−4.805
(3) 9crd + 10herc + 10q = 5fcrd + 6py + 12sill	3.1	1.12	−0.0017	−28.946
(4) 5phl + 6crd + 15herc + 15q = 5ann + 9py + 18sill	3.8	1.06	−0.0013	−34.280
(5) 3east + 3py + 4herc + 4q = 3phl + 2fcrd + 6sp	1.4	1.64	−0.0032	3.514
(6) 5naph + 6crd + 5ks + 15herc + 15q = 5ann + 9py + 5ab + 18 sill	4.0	1.08	−0.0004	−27.872

	Average pressures all end-members			excluding eastonite			The effect of varying a (H_2O) (at T = 750°C and without eastonite) a (H_2O)	$P \pm 2\sigma$	σfit
T (°C)	700	750	800	700	750	800	0.1	4.76 ± 0.9	1.14
av. P	5.0	5.4	5.7	4.7	5.1	5.4	0.3	5.06 ± 1.0	1.27
σ	0.86	0.90	0.94	0.46	0.50	0.55	0.5	5.34 ± 1.2	1.38
σfit	2.3	2.3	2.3	1.2	1.3	1.3	0.7	5.59 ± 1.2	1.49

S_2 assemblage in sample 257: g–bi–crd–sp–sill gneiss

End-members	phl	ann	east	py	alm	kp	crd	fcrd	sp	herc	q	sill
Activities (a)	0.117	0.011	0.055	0.041	0.242	0.789	0.599	0.041	0.360	0.580	1.0	1.0
σ (ln a)	0.260	0.541	0.351	0.385	0.128	0.014	0.048	0.381	0.122	0.053	0	0

Independent reactions	Calculated pressures at T = 750°C and a (H_2O) = 0.3 $P(T)$	σ	dT/dP	ln K
(1) fcrd + herc = alm + 2sill	6.3	0.63	0.0104	2.318
(2) 3crd + 3herc = 2py + alm + 6sill	5.7	0.44	0.0048	−4.616
(3) 9py + 10q + 18sill = 11crd + 5sp	5.7	0.55	0.0032	17.915
(4) 5east + 4crd = 5phl + py + 12sill	8.5	1.09	0.0099	2.622
(5) ann + crd = east + alm + 3q	4.7	1.10	0.0082	0.671

	Average pressures all end-members					excluding eastonite					The effect of varying a (H_2O) (at T = 750°C and without eastonite) a (H_2O)	$P \pm 2\sigma$	σfit
T (°C)	700	750	800	850	900	700	750	800	850	900	0.1	5.54 ± 0.7	0.56
av. P	5.7	6.1	6.4	6.7	7.0	5.7	6.0	6.3	6.6	6.9	0.3	5.97 ± 0.7	0.67
σ	0.43	0.46	0.51	0.57	0.64	0.33	0.35	0.36	0.40	0.50	0.5	6.36 ± 0.7	0.79
σfit	1.3	1.3	1.4	1.5	1.6	0.6	0.7	0.8	1.1	1.3	0.7	6.72 ± 0.7	0.90

Table 3 (*continued*)

M_2 assemblage in sample 702: opx–bi–sill symplectites

End-members	phl	ann	east	naph	crd	fcrd	py	alm	ab	ks	en	fs	mgts	q	sill
Activities (a)	0.111	0.026	0.044	0.027	0.547	0.591	0.033	0.255	0.563	0.789	0.306	0.125	0.073	1.0	1.0
σ (ln a)	0.267	0.445	0.375	0.366	0.062	0.344	0.415	0.121	0.057	0.013	0.145	0.251	0.258	0	0

Independent reactions	Calculated pressures at T = 800°C and a (H_2O) = 0.5 $P(T)$	σ	dT/dP	ln K
(1) 2py + 3q = crd + 2en	4.6	1.31	−0.0021	3.845
(2) 3crd = 2py + 5q + 4sill	6.6	0.54	0.0039	−5.007
(3) 3fcrd = 2alm + 5q + 4sill	7.1	0.64	0.0099	5.753
(4) phl + crd = east + py + 3q	3.9	1.17	−0.0015	−3.728
(5) 5naph + 6crd = 9py + 5ab + 3sill + 5H_2O	5.1	1.26	−0.0112	−11.92
(6) 5phl + 6crd = 9py + 5ks + 3sill + 5H_2O	5.2	1.25	−0.0126	−17.248
(7) 4ann + 3fcrd + 3q = 6alm + 4ks + 4H_2O	4.5	1.29	−0.0039	13.907
(8) 3east + 3fs + 3mgts + 9q = phl + 2ann + 3crd	4.5	1.39	−0.0018	12.166

	Average pressures all end-members					exluding eastonite					The effect of varying a (H_2O) (at T = 800°C and without eastonite) a (H_2O)	$P \pm 2\sigma$	σfit
T (°C)	700	750	800	850	900	700	750	800	850	900	0.1	7.25 ± 1.9	3.58
av. P	6.5	7.0	7.4	7.8	8.2	6.6	7.1	7.5	7.9	8.3	0.3	7.18 ± 1.0	1.84
σ	0.62	0.50	0.45	0.46	0.49	0.53	0.41	0.39	0.44	0.49	0.5	7.50 ± 0.78	1.49
σfit	2.5	2.0	1.7	1.8	1.9	2.1	1.6	1.5	1.7	1.8	0.7	7.79 ± 0.80	1.54

Compression along a NE-trending axis, evident as isoclinal to open, inclined F_3 and F_4 folds, resulted in the Strangways Metamorphic Complex being buried to $P = 7.5 \pm 0.8$ kbar. Cordierite in the metapelitic gneisses was partially to completely pseudomorphed by orthopyroxene + sillimanite + biotite + magnetite symplectites. The early D_3 folds appear to have been mylonitic with their fold axes parallel to the stretching lineations. Later D_3 folds are more upright and also plunge to the NE. Allen & Stubbs (1982) inferred an age of 1470 ± 60 Ma for the crystallization of symplectic aggregates similar to our M_2 symplectite. From a study of rocks in the northern Strangways Range, 50 km northwest of this study area, Warren (1982, 1983) estimated peak metamorphic pressure–temperature conditions to be 8 ± 1 kbar at 850–920°C from calculations based on a comparison of garnet + cordierite + orthopyroxene + quartz assemblages, co-existing pyroxene and clinopyroxene + plagioclase + quartz assemblages. Warren (1982, 1983) only reports fine-grained orthopyroxene + sillimanite intergrowths, which replace cordierite, after the biotite stage, as part of an isobaric cooling path. Windrum (1983) estimated similar peak metamorphic conditions of 8 kbar and 840°C for rocks from the Strangways Range. Warren (1982, 1983) postulated near isobaric cooling to the kyanite field from this 'initial' moderate-pressure metamorphic event, during which there was hydration of the high-grade assemblages: biotite formed from the hydration of orthopyroxene and garnet in felsic granulites, and pargasitic hornblende formed around the rims of orthopyroxene in metabasic rocks.

The D_4 ultramylonitization is difficult to place in this framework, but certainly pre-dates the D_5 thrusting within the Harts Range Group, and hence the "kyanite–gedrite stage" of Warren (1983). Conditions of D_4 were probably not far removed from M_2, as indicated by the neocrystallization of sillimanite and biotite and recrystallization of orthopyroxene, clinopyroxene and garnet in the ultramylonite zones.

Kyanite ± gedrite ± staurolite-bearing rocks, suggesting conditions of ~8 kbar, are observed in S-directed shear zones similar to those that bound the Ongeva Granulites and the Anamarra Granite Domain, and are assigned to the kyanite–gedrite stage (Warren 1983) (Table 1). This probably corresponds to our D_5. Later cordierite coronas on kyanite and sillimanite implies some isothermal uplift (Warren 1983) from these conditions. Pb–U zircon data yields isotopic ages of ~1750 Ma (Mortimer *et al.* 1987, Cooper *et al.* 1988) for crystallization of the Bruna Gneiss, which according to Ding & James (1985) and James and Ding (1988) intruded along a thrust contact between the Harts Range Group and the Strangways Metamorphic Complex. This data infers that thrusting occurred at ~1750 Ma and is in conflict with the ~1470 Ma dates for M_2 (Allen & Stubbs 1982). Our work shows that M_2 occurred before D_4 ultramylonitiazation and D_5 thrusting. Petrological effects of the kyanite–gedrite stage and subsequent isothermal decompression (Warren 1983) were not observed in the mineral assemblages of the discrete morphological units within the Strangways Metamorphic Complex. Hence we rely on the work of Warren (1982, 1983) for this and subsequent stages.

The tectonic setting of M_1 and M_2

Our inferred metamorphic history for the Strangways Metamorphic Complex contrasts with that of Warren (1982, 1983) and is different to the inferred metamorphic history of most granulite terrains in the world, which record evidence for either isobaric cooling or isothermal uplift (Harley 1989). An increase in pressure has been inferred for a prograde and retrograde path in

the Namaqualand Metamorphic Complex, South Africa (Waters 1986), but was explained by the addition of felsic magmas. A cooling path with a slight increase in pressure was also inferred for granulites from Labwor Hills, Uganda (Sandiford *et al.* 1987), but due to the lack of evidence for decompression the crust was assumed to be of normal thickness and the slight increase in pressure was not due to tectonism. We believe that a significant increase in pressure, at granulite-facies conditions, occurred with crustal thickening, in the Strangways Metamorphic Complex, as a result of collisional-style tectonics in the Lower to Middle Proterozoic.

Due to the extensive disruption of the Strangways Metamorphic Complex by younger retrograde shear zones and, in particular, the destruction of primary sedimentary features by recrystallization during M_1, many tectonic constraints are lost. However, M_1 has features typical of low-pressure granulite-facies metamorphisms elsewhere (e.g. Hobbs *et al.* 1984, Sandiford 1985b, Clarke *et al.* 1987, 1990) and is of a similar age to major metamorphic events in the Reynolds Range–Anmatjira Range region (Collins *et al.* in press). The events in that region are well constrained with only minor disruption to regional stratigraphy and isograds transgressing stratigraphic and deformation surfaces in each metamorphism (Clarke *et al.* 1990). Although the immediate cause of the thermally perturbed metamorphisms in the Reynolds Range–Anmatjira Range involved advection (Vernon *et al.* in press), the ultimate cause of metamorphism could probably be asthenospheric thermal perturbations (G. L. Clarke & R. Powell unpublished results). We infer a similar setting for M_1 in the Strangways Metamorphic Complex.

The up-pressure M_2 metamorphism associated with D_3 may be explained by: lithospheric loading on a thinned crust (e.g. Sandiford & Powell 1986); tectonic thickening due to overthrusting; the thrusting of the rocks deeper into the crust; or the addition of voluminous acid magmas to the crust. Given that D_3 was a major folding episode it seems likely that tectonism caused the increase in pressure. The absence of high-pressure assemblages in the Arunta Block would tend to suggest an increase in pressure due to overthrusting, rather than underthrusting in a subduction environment. Nevertheless, this increase in pressure is equivalent to a crustal thickening of 8–9 km which occurred prior to the kyanite–gedrite stage of Warren (1983). These rocks would have been near the base of a continental crust of normal thickness, or in the middle of an over-thickened crust at the end of D_2. From evidence in the Anmatjira–Reynolds Range area (Collins *et al.* in press, submitted) and the inferred isobaric cooling path from M_1, it seems likely that the M_2–D_3 event was independent of the processes responsible for M_1–D_{1-2}. If so, the M_2 metamorphism must be placed in a tectonic setting entirely unlike that inferred by Warren (1983) and quite unlike the setting for our M_1. The increase in pressure of M_2 is most similar to the effect produced by continental collision in modern orogenic belts (e.g. Selverstone *et al.* 1984).

We have no estimate of the absolute time involved between metamorphisms, nor of the time of either the D_4 ultramylonites or kyanite–gedrite stage. However, the data of Windrum & McCulloch (1986) and Mortimer *et al.* (1987) suggest only a very short period (about 150 Ma) between crustal formation and D_5 thrusting. The D_4 ultramylonites may record a continuation of the thermally-perturbed conditions that caused M_2, and could be an extensional response to crustal thickening during D_3 (c.f. Selverstone 1988, Norman 1989). However, if we accept the pressure estimate of Warren (1983) for the initial kyanite–gedrite stage, even taking errors into account, any uplift during D_4 is limited. It is conceivable that D_5 shearing is a continuation of the tectonism associated with D_3. Warren (1983) has observed cordierite overgrowths on kyanite within the D_5 shear zones which infers some isothermal uplift after the kyanite–gedrite stage probably due to isostatic adjustment of an over-thickened crust. Of course, it is entirely conceivable that either, or both, of D_4 and the kyanite–gedrite (D_5) stages are unrelated to collisional orogens and to M_2.

Acknowledgements — This work was completed whilst Tony Norman was supported by an Australian Government Commonwealth Postgraduate Research Award. Geoff Clarke and field work support for this project were funded by Australian Research Council Grant No. A38415716 (R. H. Vernon, R. H. Flood and W. J. Collins). R. H. Vernon, R. H. Flood and two anonymous reviewers are thanked for their critical comments.

REFERENCES

Allen, A. R. & Stubbs, D. 1982. An $^{40}Ar/^{39}Ar$ study of a polymetamorphic complex in the Arunta Block, central Australia. *Contr. Miner. Petrol.* **79**, 319–332.

Ashworth, J. R. 1972. Myrmekites of exsolution and replacement origins. *Geol. Mag.* **109**, 45–62.

Black, L. P., Shaw, R. D. & Stewart, A. J. 1983. Rb–Sr geochronology of Proterozoic events in the Arunta Inlier, central Australia. *Bur. Miner. Resour. J. Geol. Geophys.* **8**, 129–138.

Caby, R., Pecher, A. & Lefort, P. 1983. Le grand chevauchement central Himalayen: nouvelle donnees sur le metamorphism inverse á la base de la dalle du Tibet. *Rev. Géogr. phys. Géol. dyn.* **24**, 89–100.

Clarke, G. L., Burg, J. P. & Wilson, C. J. L. 1986. Structural and stratigraphic constraints on the Proterozoic tectonic history of the Olary Block, South Australia. *Precambrian Res.* **34**, 107–137.

Clarke, G. L., Guiraud, M., Powell, R. & Burg, J. P. 1987. Metamorphism in the Olary Block, South Australia: compression with cooling in a Proterozoic fold belt. *J. metamorph. Geol.* **5**, 291–306.

Clarke, G. L., Collins, W. J. & Vernon, R. H. 1990. Successive overprinting granulite facies metamorphic events in the Anmatjira Ranges, central Australia. *J. metamorph. Geol.* **8**, 65–88.

Clarke, G. L., Powell, R. & Guiraud, M. 1989. Low-pressure granulite facies metapelitic assemblages and corona textures from Mac-Robertson Land, East Antarctica: the importance of Fe_2O_3 and TiO_2 in accounting for spinel-bearing assemblages. *J. metamorph. Geol.* **7**, 323–335.

Collins, W. J., Williams, I. S. & Compston, W. In press. Three short-lived granulite facies events in the Arunta Block, central Australia. *Geology*.

Collins, W. J., Vernon, R. H. & Clarke, G. L. Submitted. Two discrete structural terranes in the Anmatjira Range, central Australia. *J. Struct. Geol.*

Collins, W. J. & Teyssyier, C. 1989. Crustal scale ductile fault systems in the Arunta Inlier, central Australia. *Tectonophysics* **158**, 49–66.

Cooper, J. A., Mortimer, G. E. & James, P. R. 1988. Rate of Arunta Inlier evolution at the eastern margin of the Entia Dome, Central Australia. *Precambrian Res.* **40/41**, 217–232.

Ding, P. & James, P. R. 1985. Structural evolution of the Harts Range area and its implication for the development of the Arunta Block, central Australia. *Precambrian Res.* **27**, 251–276.

Ellis, D. J., 1987. Origin and evolution of granulites in normal and thickened crust. *Geology* **15**, 167–170.

England, P. C. 1987. Diffuse continental deformation: length scales, rates and metamorphic evolution. In: *Tectonic Settings of Regional Metamorphism* (edited by Oxburgh, E. R., Yardley, B. W. D. & England, P. C.). The Royal Society. Cambridge University Press, London, 3–22.

England, P. C. & Richardson, S. W. 1977. The influence of erosion on the mineral facies of rocks from different metamorphic environments. *J. geol. Soc. Lond.* **134**, 201–213.

Harley, S. L. 1984. The solubility of Alumina in orthopyroxene coexisting with garnet in FeO–MgO–Al_2O_3–SiO_2 and CaO–FeO–MgO–Al_2O_3–SiO_2. *J. Petrol.* **25**, 665–696.

Harley, S. L. 1989. The origin of granulites: a metamorphic perspective. *Geol. Mag.* **126**, 215–331.

Hensen, B. J. 1971. Theoretical phase relations involving cordierite and garnet in the system MgO–FeO–Al_2O_3–SiO_2. *Contr. Miner. Petrol.* **3**, 191–214.

Hensen, B. J. & Green, D. H. 1973. Experimental study of the stability of cordierite and garnet in pelitic compositions at high pressures and temperatures. III. Synthesis of experimental data and geological applications. *Contr. Miner. Petrol.* **38**, 151–166.

Hobbs, B. E., Archibald, N. J., Etheridge, M. A. & Wall, V. J. 1984. Tectonic history of the Broken Hill Block, Australia. In: *Precambrian Tectonics Illustrated* (edited by Kroner, A. & Greiling, R.) E. Schweizerbart'sche Verlagsbuchhandlung, Stuttgart, 353–368.

Holland, T. J. B. & Powell, R. 1990. An internally consistent dataset with uncertainties and correlations: 4. *J. metamorph. Geol.* **8**, 89–124.

Iyer, S. S., Woodford, P. J. & Wilson, A. F. 1976. Rb–Sr isotopic studies of a polymetamorphic granulite terrain, Strangways Range, central Australia. *Lithos* **9**, 211–224.

James, P. R. & Ding, P. 1988. Caterpillar tectonics in the Harts Range area: a kinship between two sequential Proterozoic extension-collision orogenic belts within the eastern Arunta Inlier of central Australia. *Precambrian Res.* **40/41**, 199–216.

Joklik, G. F. 1955. The geology and mica fields of the Harts Range, central Australia. *Bull. Bur. Miner. Resour.* **26**.

Lefort, P., 1975. Himalayas: the collided range. Present knowledge of the continental arc. *Am. J. Sci.* **275A**, 1–44.

Mortimer, G. E., Cooper, J. A. & James, P. R. 1987. U–Pb and Rb–Sr geochronology and geological evolution of the Harts Range ruby mine area of the Arunta inlier, central Australia. *Lithos* **20**, 445–467.

Noakes, L. C. 1953. The structure of the Northern Territory in relation to mineralization. *Proc. 5th Empire Mineral Congress, Geology of Australian Ore Deposits*, 284–296.

Norman, A. R., 1989. Ultramylonite zones transecting high-grade Proterozoic rocks of the Strangways Orogenic Belt. *Geol. Soc. Aust.* (Abs.) **24**, 104–105.

Oliver, R. L., Lawrence, R. W., Ding, P., Bowyer, D. G., Goscombe, B. D. & Sivell, W. J. 1988. Metamorphism and crustal considerations in the Harts Range and neighbouring regioins, Arunta inlier, central Australia. *Precambrian Res.* **40/41**, 277–296.

Paterson, S. R., Vernon, R. H. & Tobisch, O. T. 1989. A review of criteria for the identification of magmatic and tectonic foliations in granitoids. *J. Struct. Geol.* **11**, 349–363.

Phillips, G. N. & Wall, V. J. 1981. Evaluation of prograde regional metamorphic conditions: their implications for the heat source and water activity during metamorphism in the Willyama Complex, Broken Hill, Australia. *Bull. Mineral.* **104**, 801–810.

Powell, R. & Holland, T. J. B. 1988. An internally consistent dataset with uncertainties and correlations: 3. Applications to geobarometry, worked examples and a computer program. *J. metamorph. Geol.* **6**, 173–204.

Richardson, S. W. 1968. Staurolite stability in a part of the system Fe–Al–Si–O–H. *J. Petrol.* **9**, 467–488.

Sandiford, M. 1985a. The origin of retrograde shear zones in the Napier Complex: implications for the tectonic evolution of Enderby Land, Antarctica. *J. Struct. Geol.* **7**, 477–488.

Sandiford, M. 1985b. The metamorphic evolution of granulites at Fyfe Hills: implications for Archaean crustal thickness in Enderby Land, Antarctica. *J. metamorph. Geol.* **3**, 155–178.

Sandiford, M. In press. Secular trends in the thermal evolution of metamorphic terrains. *Earth Planet. Sci. Lett.*

Sandiford, M., Neall, F. B. & Powell, R. 1987. Metamorphic evolution of aluminous granulites from Labwor Hills, Uganda. *Contr. Miner. Petrol.* **95**, 217–225.

Sandiford, M. & Powell, R. 1986. Deep crustal metamorphism during continental extension: ancient and modern examples. *Earth Planet. Sci. Lett.* **79**, 151–158.

Selverstone, J. 1988. Evidence for east–west crustal extension in the eastern Alps: implications for the unroofing history of the Tauern Window. *Tectonics* **7**, 87–105.

Selverstone, J., Spear, F. S., Franz, G. & Morteani, G. 1984. High-pressure metamorphism in the SW Tauern Window, Austria: *P–T* paths from hornblende–kyanite–staurolite schists. *J. Petrol.* **25**, 501–531.

Shackleton, R. M. & Reis, A. C. 1984. The relation between regionally consistent stretching lineations and plate motions. *J. Struct. Geol.* **6**, 111–117.

Shaw, R. D. & Langworthy, A. P. 1984. Geology of the Strangways Range region, Northern Territory. Bureau of Mineral Resources, Australia. 1:100,000 map commentary.

Shaw, R. D., Langworthy, A. P., Offe, L. A., Stewart, A. J., Allen, A. R. & Senior, B. R. 1979. Geological report on 1:100,000-scale mapping the southeastern Arunta Block, Northern Territory. *Bur. Miner. Resour. Geol. Geophys. Rec.* **1979/47**.

Shaw, R. D., Stewart, A. J. & Rickard, M. J. 1984. Geology of the Arltunga–Harts Range region, Northern Territory. Bureau of Mineral Resources, Australia. 1:100,000 map commentary.

Simpson, C. & Schmid, S. M. 1983. An evaluation of criteria to deduce the sense of movement in sheared rocks. *Bull. geol. Soc. Am.* **94**, 1281–1288.

Stewart, A. J. 1971. Potassium-argon dates from the Arltunga Nappe Complex, Northern Territory. *J. geol. Soc. Aust.* **17**, 205–211.

Stewart, A. J., Shaw, R. D. & Black, L. P. 1984. The Arunta Inlier, a complex ensialic mobile belt in central Australia. Part 1: Stratigraphy, correlations and origin. *Aust. J. Earth Sci.* **31**, 445–455.

Stüwe, K. & Powell, R., 1989a. Metamorphic evolution of the Bunger Hills, east Antarctica: evidence for substantial post-metamorphic peak compression with minimal cooling in a Proterozoic orogenic event. *J. metamorph. Geol.* **7**, 449–464.

Stüwe, K. & Powell, R. 1989b. Low-pressure granulite facies metamorphism in the Larsemann Hills area, East Antarctica; petrology and tectonic implications for the evolution of the Prydz Bay area. *J. metamorph. Geol.* **7**, 465–484.

Thompson, A. B. & Ridley, J. R. 1987. Pressure–temperature–time (*P–T–t*) histories of orogenic belts. *Phil. Trans. R. Soc. London. A321*, 27–45.

Turner, F. J., 1968. *Metamorphic Geology*. McGraw–Hill, London.

Vernon, R. H., Clarke, G. L. & Collins, W. J. In press. Very low-pressure granulite facies metamorphism and melting, Mt Stafford, central Australia. In: *High Temperature Metamorphism and Crustal Anatexis* (edited by Ashworth, J. R. & Brown, M.). *Spec. Publ. Mineral. Soc.* Unwin-Hyman, London.

Warren, R. G. 1982. Metamorphic paragenesis in part of the Arunta Complex, Northern Territory. Unpublished PhD. thesis, University of New South Wales.

Warren, R. G. 1983. Metamorphism and tectonic evolution of granulites, Arunta Block, central Australia. *Nature* **305**, 300–303.

Warren, R. G. & Stewart, A. J. 1988. Isobaric cooling of Proterozoic high-temperature metamorphites in the northern Arunta Block, central Australia: implications for tectonic evolution. *Precambrian Res.* **40/41**, 175–198.

Waters, D. J. 1986. Metamorphic zonation and thermal history of pelitic gneisses from western Namaqualand, South Africa. *Trans. geol. Soc. S. Afr.* **89**, 97–102.

Wells, P. R. A. 1980. Thermal models for the magmatic accretion and subsequent metamorphism of continental crust. *Earth Planet. Sci. Lett.* **46**, 253–265.

Windley, B. F. 1985. Metamorphism and tectonics of the Himalaya. *J. geol. Soc. Lond.* **140**, 849–865.

Windrum, D. P. 1983. Chemical and thermal evolution of Strangways granulites, central Australia. PhD thesis, The Australian National University, Canberra.

Windrum, D. P. & McCulloch, M. T. 1986. Nd and Sr isotopic systematics of central Australian granulites: chronology of crustal development and constraints on the evolution of lower continental crust. *Contr. Miner. Petrol.* **94**, 289–303.